Nonlinear peristaltic waves: a bitter pill to swallow

Daisuke Takagi

September 28, 2009

Abstract

Nonlinear waves of fluid are driven in an elastic tube by imposing a radial force of sinusoidal form. The governing equations of the deformation of the tube and the flow rate inside the tube are derived using linear elasticity theory and lubrication theory. Steady and periodic solutions in the reference frame of a steadily propagating wave are obtained by either asymptotic theory in the two limits of small and large forcing amplitudes or numerical techniques for moderate forcing amplitudes. A strongly deformed tube of Newtonian fluid is shown to feature an occluded region and a peak region, which depends importantly on the elastic properties of the tube and weakly on the large forcing amplitude. The flow rate inside the tube reduces significantly when the fluid has a yield stress, as investigated using a Bingham plastic model. The flow of Newtonian fluid containing a rigid rod in the tube shows that a maximal speed of the rod is attained by imposing a radial force of moderate amplitude. The rod generally declines in speed with increasing radius, suggesting that the python, which must take in food by peristalsis without grinding into smaller pieces, has a bitter pill to swallow.

1 Introduction

Fluid inside a deformable tube can be driven by the mechanism of peristaltic action. Many biological ducts convey contents, including a bolus in the gastronomical duct and urine in the ureter, by propagating waves of muscular contraction and relaxation. A python is able to swallow prey of considerable size this way. A related type of flow in a deformed tube occurs in peristaltic pumps, which are used for the infusion of medication into the circulatory system and the treatment of wastewater in the environment, amongst many other applications. Pushing toothpaste out of its tube is another example of relevance.

Mathematical models of peristaltic motion can be developed using lubrication theory, provided that effects due to fluid inertia are negligible. The low-Reynolds-number flow of Newtonian fluid was described in an axisymmetric tube with either a sinusoidal (Shapiro et al., 1969) or non-sinusoidal (Lykoudis and Roos, 1970) deformation in its radius. The flow of non-Newtonian fluid

was studied in a similar fashion, given a small deformation in the tube radius (Frigaard and Ryan, 2004; Vajravelu et al., 2005). Another variation is to introduce a peripheral layer of Newtonian fluid adjacent to the wall, which has a different viscosity from that of the inner fluid (Brasseur et al., 1987). These models prescribe the tube deformation without taking elastic properties of the tube into consideration.

Of interest is a situation where the shape of the tube is unknown a priori and must be solved as part of the problem, given some coupling between the hydrodynamics and the mechanics of the elastic tube. Related free-boundary problems of flow near an elastic material arise in a range of contexts, including the swimming of a microorganism near a rigid wall (Argentina et al., 2007; Balmforth et al., 2009) and premelting of ice in a deformable capillary (Wettlaufer and Worster, 1995; Wettlaufer et al., 1996). In the context of peristaltic motion with a prescribed activation wave of muscular contraction, where elastic tubes result in finite-amplitude deformations, tubes containing Newtonian fluid (Carew and Pedley, 1997) and a rigid bolus (Bertuzzi et al., 1983) have been solved numerically. Analytic solutions are desirable for gaining a deeper understanding of peristaltic flow inside a strongly deformed tube, where the response in tube radius is a nonlinear function of the forces driving the flow.

Here, theoretical models of peristaltic flow are developed, given a sinusoidal wave of radial force of arbitrary amplitude that translates along an elastic tube. In the reference frame of the wave, steady and periodic solutions are obtained to describe the motion of three different materials inside the tube. In section 2, the flow of Newtonian fluid is investigated inside a linearly elastic tube and separately inside a tube of finite bending stiffness. In section 3, the flow governed by a Bingham plastic model is considered, which exhibits the dual behaviour of a fluid and a solid. Familiar examples of non-Newtonian fluid described by the Bingham model include mud, paint, slurry, and toothpaste. In section 4, the propulsion of a rigid body in a Newtonian fluid is examined. The coupled motion of the solid and the fluid provides useful insight into the flow of pills in the gastronomical duct, kidney stones in the ureter, and blood cells in small blood vessels. In each section, the governing equations are derived and solved using asymptotic theory in the two limits of small and large forcing amplitudes, which give rise to linear and nonlinear responses in tube radius respectively. The theoretical results are complemented by numerical solutions that describe responses to moderate forcing amplitudes.

2 Newtonian fluid

Consider a Newtonian fluid of density ρ and dynamic viscosity μ with pressure p_0, inside a cylindrical tube of constant radius R in its undeformed state. A radial force per unit area of sinusoidal form $F(z-ct) = \eta \sin[(z-ct)2\pi/L]$ is applied on the tube along the axial coordinate z at time t. The imposed force, characterised by its amplitude η, steady speed c, and wavelength L, perturbs the pressure p inside the tube and the tube radius a, as sketch in figure 1. The

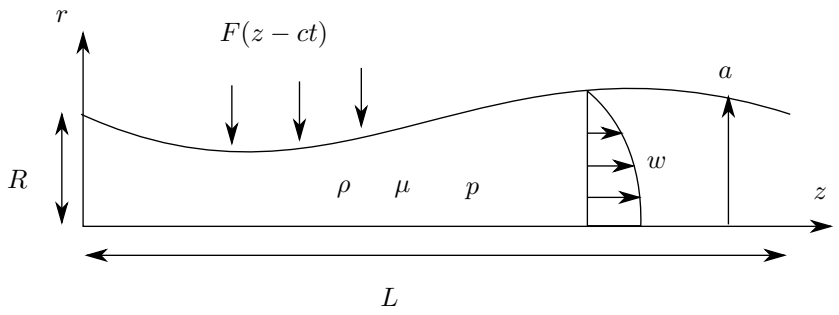

Figure 1: Schematic sketch in cylindrical polar coordinates of a deformed tube filled with Newtonian fluid. A prescribed radial force F perturbs the tube of radius a and induces flow with axial velocity w.

velocity $\mathbf{u}$ of the induced flow of fluid is governed by

$$\rho\frac{D\mathbf{u}}{Dt} = -\nabla p + \mu\nabla^2\mathbf{u}, \tag{1}$$

subject to the condition of incompressibility,

$$\nabla\cdot\mathbf{u} = 0. \tag{2}$$

The elastic properties of the tube are such that the change in pressure across the tube is of the form

$$\Delta p|_{r=a} = D\frac{\partial^n}{\partial z^n}(a-R) + F, \tag{3}$$

where $n = 0, 4$ characterises the type of elastic material constituting the tube and D denotes its stiffness. The case of $n = 0$ corresponds to a linearly elastic tube such that its deformation is proportional to the net radial force. For example, the tube could be attached by springs to a rigid surrounding backing, where D is the spring constant. The case of $n = 4$ corresponds to a thin shell of bending stiffness $D = h^3E/12(1-\nu^2)$, where h is the shell thickness, E the Young modulus and ν the Poisson ratio (Love, 1944). The objective is to determine the shape of the tube and the volumetric flow rate q per wave period, L/c.

It is convenient to introduce dimensionless variables of axial coordinate $z' = z/L$, radial coordinate $r' = r/R$, time $t' = tc/L$, pressure $p' = pR/\mu c$, tube stiffness $D' = DR/\mu c$, amplitude of forcing $\eta' = \eta R/\mu c$, and flow rate $q' = q/\pi R^2 c$. All quantities from here onwards are dimensionless, without the primes for simplicity. In addition, it is convenient to formulate the problem in the reference frame of the wave, moving at speed 1 in the z direction. The advantage of moving with the wave is that the tube radius is steady in time in this reference frame, as justified below. The axial velocity w and radial velocity u are governed by (1)

$$\delta^2 Re\frac{Du}{Dt} = -\frac{\partial p}{\partial r} + \delta^2\frac{1}{r}\frac{\partial}{\partial r}\left(r\frac{\partial u}{\partial r}\right) + \delta^4\frac{\partial^2 u}{\partial z^2} \tag{4}$$

and

$$Re\frac{Dw}{Dt} = -\frac{\partial p}{\partial z} + \frac{1}{r}\frac{\partial}{\partial r}\left(r\frac{\partial w}{\partial r}\right) + \delta^2\frac{\partial^2 w}{\partial z^2}, \tag{5}$$

where

$$\delta \equiv \frac{R}{L} \tag{6}$$

is the aspect ratio of the region of interest and

$$Re \equiv \frac{\rho c R^2}{\mu L} \tag{7}$$

is the Reynolds number. The deformation of the tube is small provided that $\delta \ll 1$ under the long-wave approximation. Inertia is negligible compared to viscous forces provided that $Re \ll 1$. It is natural to seek steady solutions in the wave frame because the explicit dependence on time is dropped by neglecting effects due to inertia. Under these approximations of lubrication theory, the leading-order equation of (4) indicates that the pressure inside the tube is uniform in the radial direction. Consequently, $\Delta p|_{r=a} = p - p_0$ so

$$\frac{dp}{dz} = D\frac{d^{1+n}a}{dz^{1+n}} + \eta\cos z, \tag{8}$$

by differentiating (3) with respect to z. The leading-order equation of (5) gives rise to a second-order differential equation for the axial velocity w,

$$\frac{dp}{dz} = \frac{1}{r}\frac{\partial}{\partial r}\left(r\frac{\partial w}{\partial r}\right). \tag{9}$$

The associated boundary conditions are $w = -1$ on $r = a$, by the condition of no slip on the tube wall, and $\partial w/\partial r = 0$ on $r = 0$, by either regularity or axisymmetry of the flow. Note that $w = -1$ in the wave frame corresponds to no axial flow in the lab frame. Integrating (9) twice and imposing the two boundary conditions yield the velocity profile in the wave frame,

$$w = \frac{1}{4}\frac{dp}{dz}(r^2 - a^2) - 1. \tag{10}$$

Streamlines are determined by contours of the streamfunction

$$\psi = -\frac{1}{16}\frac{dp}{dz}r^2(2a^2 - r^2) - \frac{1}{2}r^2, \tag{11}$$

which is obtained by integrating $w = r^{-1}\partial\psi/\partial r$.

A measure of the proportion of fluid propagating with a wave is given by the time-averaged flow rate in the lab frame, denoted by q. The flow rate in the lab frame at any axial coordinate is obtained by integrating the axial velocity in the lab frame over the cross-section of the tube, $2\int_0^a (w+1)r\,dr$. Its average in time, which is equivalent to its average in z over 2π, is computed by using (10) and the global conservation of fluid volume

$$\langle a^2 \rangle = 1, \tag{12}$$

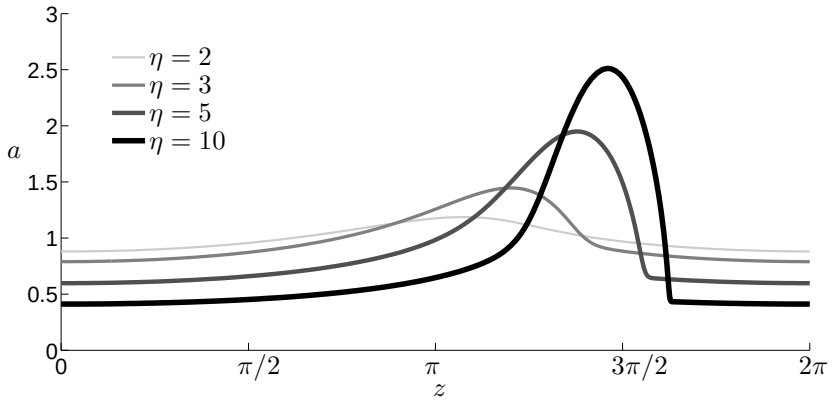

Figure 2: Numerical solutions of the tube radius perturbed by different forcing amplitudes η. The tube is of type $n = 0$ and has stiffness $D = 1$. As η increases, the deformation of the tube increases.

where $\langle\cdot\rangle \equiv (2\pi)^{-1}\int_0^{2\pi}\cdot\, dz$. The time-averaged flow rate in the lab frame is given by

$$q = -\frac{1}{8}\frac{dp}{dz}a^4 - a^2 + 1, \tag{13}$$

where dp/dz is given by (8). When $n = 0$ in (8), the first-order differential equation (13) must be solved subject to the periodic boundary condition $a(0) = a(2\pi)$. When $n = 4$ in (8), the fifth-order differential equation (13) must be solved subject to periodic boundary conditions $d^i a/dz^i(0) = d^i a/dz^i(2\pi)$ for $i = 0, 1, 2, 3, 4$. A boundary-value problem with an eigenvalue to be determined, q, must be solved to determine the radius of the tube.

The system of equations, (12) and (13), can be solved numerically using a built-in function of Matlab called bvp4c. The forcing amplitude η is incremented slowly from 0 with $a = 1$ to obtain a solution during each iteration, which forms an initial guess for solutions with successive increments of η. A representative set of solutions for the tube radius in response to different forcing amplitudes η is plotted in figure 2. The associated solutions of the eigenvalue q are presented later. For small η, the tube deformation is small as expected. As η increases, the tube is occluded except near $z = 3\pi/2$, where its radius peaks due to the imposed force that is maximal and radially outward. Streamlines of the flow induced with forcing amplitudes $\eta = 2$ and $\eta = 3$ are shown in figures 3 and 4, obtained using equation (11). As η increases, a qualitative change in the structure of the streamlines is observed, from axial flow that is everywhere negative in the wave frame to the development of a recirculating zone where the tube peaks in radius. Fluid inside the recirculating zone propagates with the wave.

In the limit as $\eta \to 0$, the tube is almost undeformed and flow inside the tube is expected to be negligible. In the limit as $\eta \to \infty$, the trapped core near

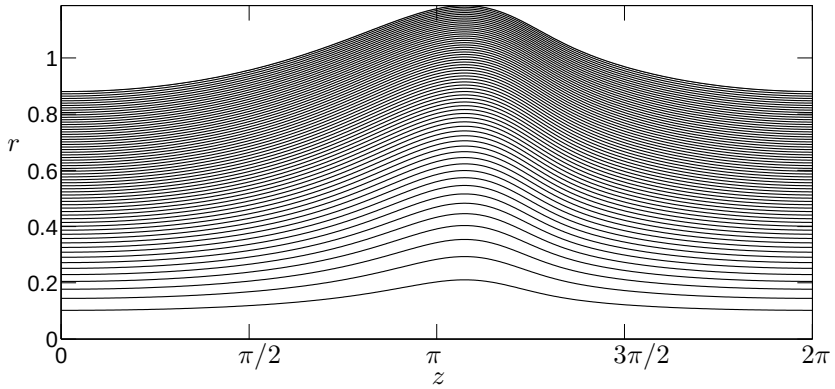

Figure 3: Streamlines of flow driven by a radial force of amplitude $\eta = 2$. In the wave frame, the axial velocity inside the tube is everywhere negative.

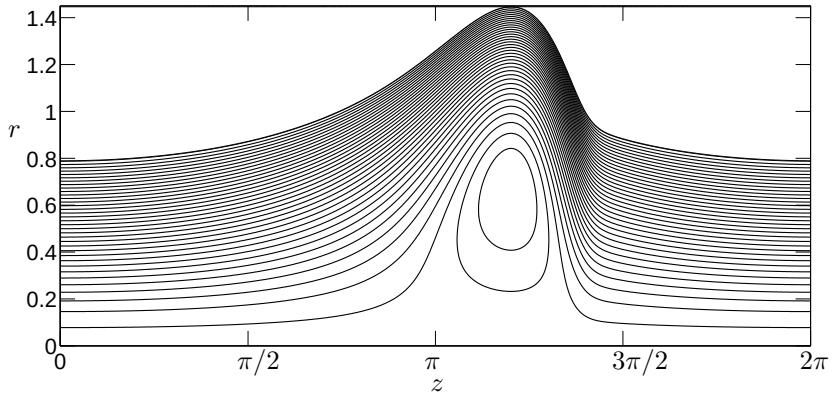

Figure 4: Streamlines of flow driven by a radial force of amplitude $\eta = 3$. In the wave frame, a trapped core, recirculating anti-clockwise, forms in the region where a peak radius of the tube is attained.

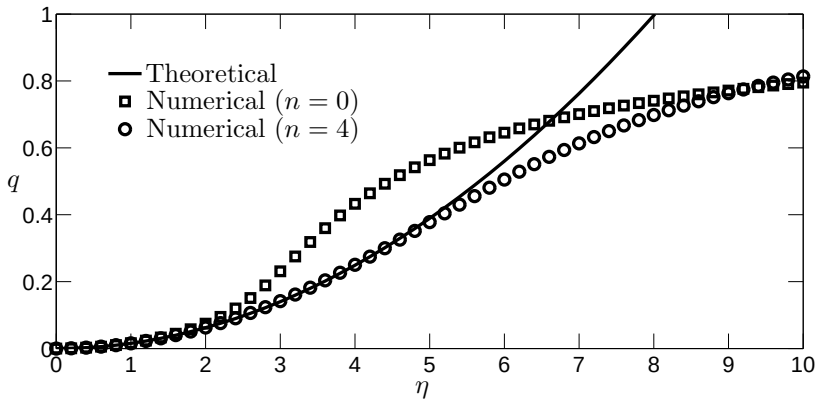

Figure 5: Theoretical prediction and numerical solutions of the time-averaged flow rate in the lab frame for small forcing amplitudes η. The numerical solutions are obtained with tube stiffness $D = 1$ and agree with the theoretical prediction in the asymptotic limit as $\eta \to 0$, independent of the type of tube, $n = 0, 4$.

$z = 3\pi/2$ is expected to increase in size and allow most of the fluid in the tube to propagate with the wave. The two limits of small and large η are investigated separately using asymptotic theory.

In the small-amplitude limit, $\eta \ll 1$, it is fruitful to seek series solutions of a and q about the base state, $a = 1$ and $q = 0$. The subsequent term in a is of order η, which indicates that the leading term in q is of order η^2, by operating $\langle\cdot\rangle$ on (13) and using the integral constraint (12). The radius of the tube responds linearly to the amplitude of the external forcing. Substituting $a = 1 + \eta a_1 + o(\eta^2)$ into (13) gives

$$D\frac{d^{1+n}a_1}{dz^{1+n}} - 16a_1 = \cos z, \tag{14}$$

which is solved subject to periodic boundary conditions. The solution is given by

$$a = 1 - \eta\frac{16\cos z - D\sin z}{16^2 + D^2} + o(\eta^2), \tag{15}$$

independent of the type of tube characterised by $n = 0, 4$ because $\sin z$ and $\cos z$ are invariant under four differentiations. Operating $\langle\cdot\rangle$ on (13), which gives $q = -\langle(dp/dz)a^4/8\rangle$, and imposing periodic boundary conditions at $z = 0, 2\pi$, yield an expression for the time-averaged flow rate,

$$q = \frac{4\eta^2}{16^2 + D^2} + o(\eta^3), \tag{16}$$

which is in agreement with numerical results for small η as shown in figure 5. Note that the theoretical prediction given by (16) in the asymptotic limit as $\eta \to 0$ agrees with numerical results up to $\eta \approx 2$ inside a tube of type $n = 0$

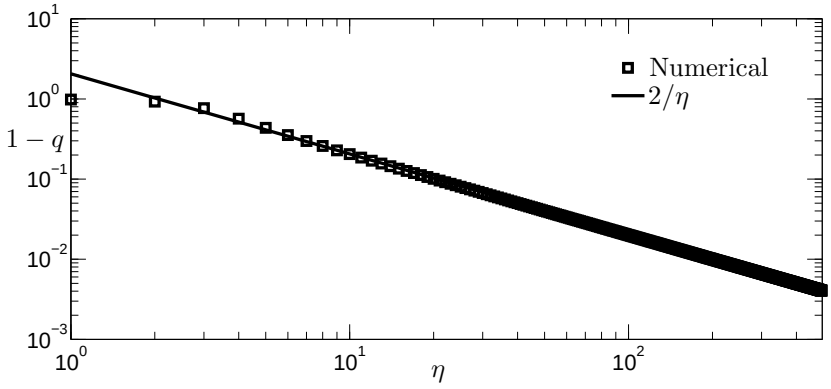

Figure 6: Theoretical prediction and numerical solutions of the characteristic proportion of fluid left behind the wave for large η, plotted on logarithmic scales. The tube is of type $n = 0$ and has stiffness $D = 1$.

and up to $\eta \approx 5$ inside a tube of type $n = 4$. The numerical results in the figure suggest that q approaches 1 as η increases, which is investigated below.

In the large-amplitude limit, $\eta \gg 1$, two qualitatively distinct regions develop, one near $z = 3\pi/2$ where the tube radius peaks, and the other away from $z = 3\pi/2$ where the tube is occluded. Quantitative details of the two regions must be considered separately in the two types of tubes, $n = 0$ and $n = 4$. Of interest is the quantity $1 - q$, a measure of the proportion of fluid left behind the wave.

When $n = 0$, the tube radius is expected to approach 0 in the occluded region so the dominant contribution to dp/dz in (13) arises from the second rather than the first term on the right hand side of (8). The governing differential equation (13) reduces to an algebraic equation

$$-\eta \cos z \, a^4 - 8a^2 + (1 - q) = 0. \tag{17}$$

This quadratic equation in a^2 results in two branches,

$$a^2 = \frac{4}{\eta \cos z} \left(-1 \pm \sqrt{1 + \frac{\eta}{2}(1 - q) \cos z} \right), \tag{18}$$

where $\pm$ is either positive in the lower branch or negative in the upper branch. Only the lower branch corresponds to a real tube radius throughout the domain $0 \le z \le 2\pi$. However, its gradient is unphysically discontinuous at $z = \pi$, which must be resolved by switching smoothly to the upper branch. The condition that the lower and upper branches meet at $z = \pi$ requires

$$q = 1 - 2\eta^{-1} + o(\eta^{-2}). \tag{19}$$

The theoretical prediction for the flow rate given by (19) is in excellent agreement with numerical results, as shown in figure 6. Note that the characteristic

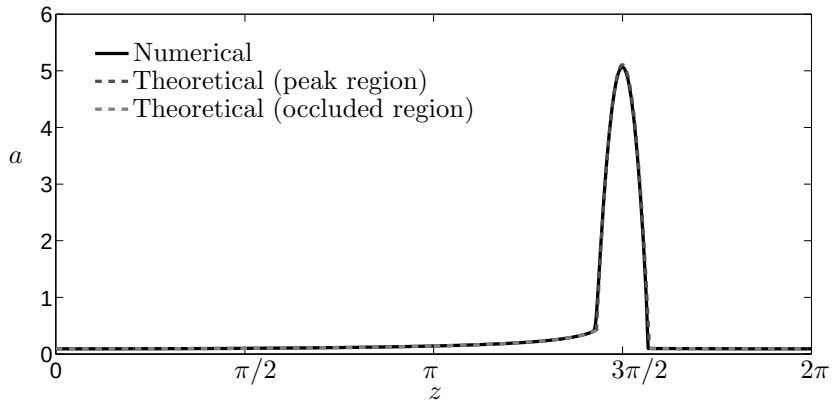

Figure 7: Theoretical and numerical solutions of the tube radius deformed with forcing amplitude $\eta = 200$. The theoretical solution, given by (21) in the peak region and (20) in the occluded region, is in excellent agreement with the numerical solution obtained using input parameters $n = 0$ and $D = 1$.

proportion of fluid left behind the wave is determined solely by the occluded region, independent of the peak region to be examined later. Substituting (19) into (18) gives the solution for the tube radius in the occluded region,

$$a = \begin{cases} 2\left(1 - \sqrt{2}|\cos z/2|\right)^{-1/2}\eta^{-1/2} + o(\eta^{-1}) & \pi \le z < 3\pi/2, \\ 2\left(1 + \sqrt{2}|\cos z/2|\right)^{-1/2}\eta^{-1/2} + o(\eta^{-1}) & 0 \le z < \pi,\ 3\pi/2 < z \le 2\pi, \end{cases} \tag{20}$$

which is continuous at $z = \pi$ but discontinuous at $z = 3\pi/2$. The radius of the tube diverges as $z \to 3\pi/2$ from below and converges to $\sqrt{2/\eta}$ from above. The divergence and discontinuity represent the formation of a shock, which is resolved mathematically by considering a boundary layer near $z = 3\pi/2$, the peak region.

In the peak region, the tube radius is expected to grow arbitrarily with forcing amplitude η, suggesting that only the first term on the right hand side of (13) is dominant. This means that $dp/dz = 0$ so the pressure in the peak region is uniform. It can be shown, by combining equations (8) and (12), where $\cos z$ in (8) is expanded near $z = 3\pi/2$, that the rescaled tube radius is given by $A = \eta^{-1/5}a$ and has a peak A_{max} at $\zeta = 0$, where ζ is the rescaled axial coordinate in the peak region such that $z = 3\pi/2 + \eta^{-2/5}\zeta$. The rescaled equation of (8) reduces to $D\,dA/d\zeta + \zeta = 0$ and is integrated to obtain

$$A = A_{max} - \frac{\zeta^2}{2D}. \tag{21}$$

The tube radius in the peak region has a parabolic profile, provided that the tube has stiffness $D > 0$. The peak radius of the tube is given by $a_{max} = \eta^{1/5}A_{max}$

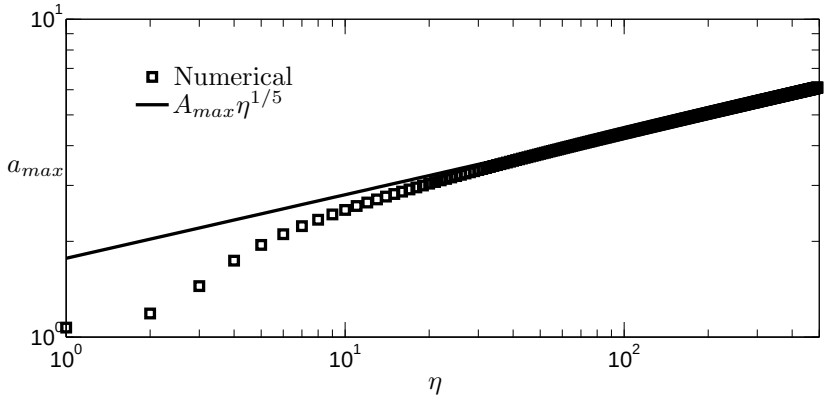

Figure 8: Theoretical prediction and numerical solutions of the peak radius of the tube of type $n = 0$ and stiffness $D = 1$, plotted on logarithmic scales.

with

$$A_{max} = \left(\frac{15^2\pi^2}{2^7 D^5}\right)^{1/5}, \tag{22}$$

which is obtained by solving the rescaled equation of (12), $\int_{-\delta}^{\delta} A^2\, d\zeta = 2\pi$, where $\delta = \sqrt{2DA_{max}}$ corresponds to the half-width of the peak region. The occluded region given by (20) and the peak region given by (21) agree with numerical results, demonstrated in figure 7 for a tube of stiffness $D = 1$, forced with amplitude $\eta = 200$. The scaling $\eta^{1/5}$ and the prefactor (22) for the peak radius of the tube also agree with numerical results as shown in figure 8. The form of a_{max} indicates that the peak radius depends importantly on the tube stiffness but depends weakly on the forcing amplitude for large η.

When the type of tube is characterised by $n = 4$, different scalings of the flow are obtained in both the occluded and peak regions. In the peak region, the pressure is uniform and the rescaled equations are obtained by combining equations (8) and (12), as before. The rescaled tube radius is given by $A = \eta^{-1/13}a$ and satisfies $D\, d^5A/d\zeta^5 + \zeta = 0$, subject to the boundary conditions that A, $dA/d\zeta$, and $d^2A/d\zeta^2$ all vanish near the ends of the peak region, as $\zeta \to \pm\delta$, where $z = 3\pi/2 + \eta^{-2/13}\zeta$. These boundary conditions ensure that the peak region matches smoothly to the occluded region, which is considered later. Integrating the fifth-order differential equation fives times gives the radius of the tube in the peak region,

$$a = \eta^{1/13}\frac{1}{6!D}\left(\delta^2 - \zeta^2\right)^3, \tag{23}$$

where

$$\delta = (\pi D^2 6!^2)^{1/13}\left(\frac{11}{3} - \frac{20}{7} - \frac{6}{11} + \frac{1}{13}\right)^{-1/13} \tag{24}$$

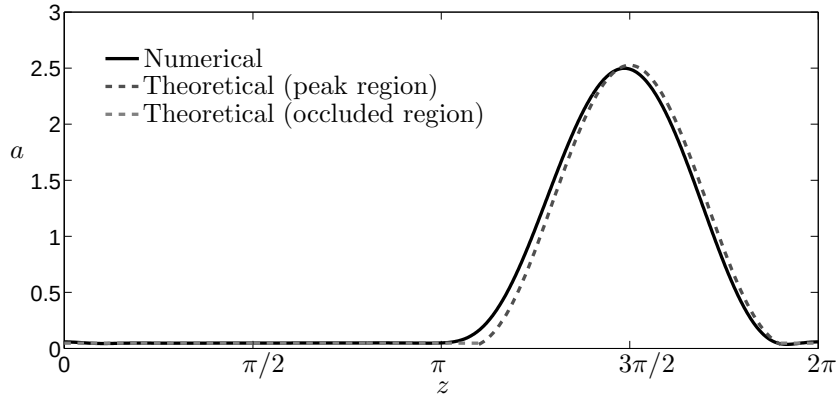

Figure 9: Theoretical and numerical solutions of the tube radius deformed with forcing amplitude $\eta = 200$. The theoretical prediction, given by (23) in the peak region, agrees with the numerical solution obtained using input parameters $n = 4$ and $D = 1$.

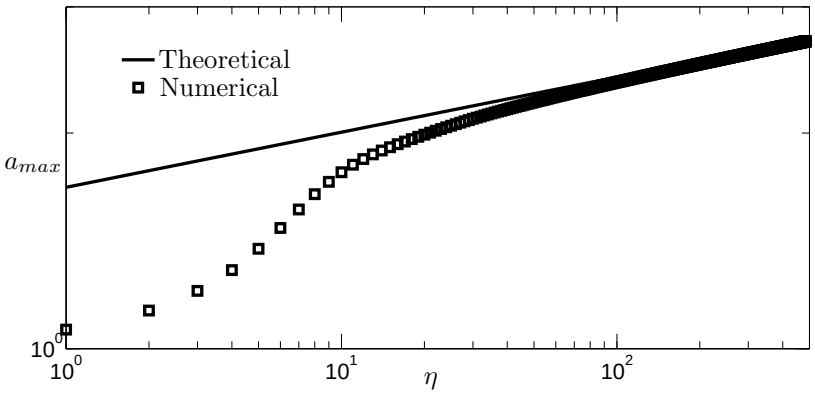

Figure 10: Theoretical prediction and numerical solutions of the peak radius of the tube of type $n = 4$, plotted on logarithmic scales.

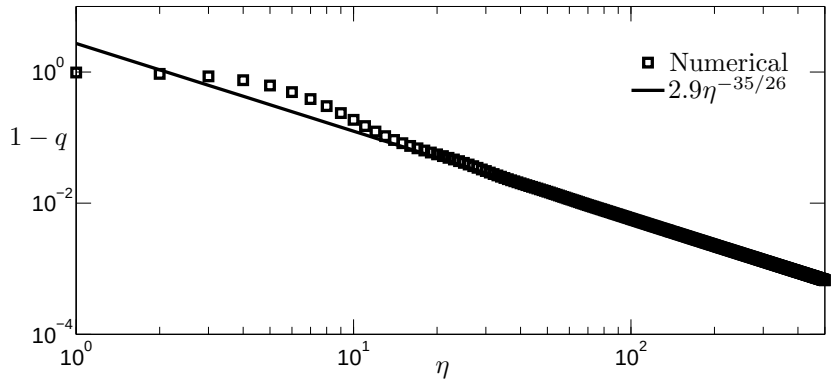

Figure 11: Theoretical prediction and numerical solutions of the characteristic proportion of fluid left behind the wave inside a tube of type $n = 4$, plotted on logarithmic scales.

is obtained using the rescaled integral constraint (12), $\int_{-\delta}^{\delta} A^2\, d\zeta = 2\pi$. The peak region agrees with numerics, demonstrated by figure 9 for $\eta = 200$, $D = 1$. The maximal radius of the tube at $z = 3\pi/2$, $\eta^{1/13}\delta^6/6!D$, agrees with the numerics as shown in figure 10. Note that the forcing amplitude must increase by thirteen orders of magnitude to deform the tube radius by one order of magnitude. A comparison of figures 7 and 9 indicates that for the same value of D and large η, the peak region of the tube of type $n = 4$ is longer and less deformed than that of the tube of type $n = 0$. The extremely weak dependence of the tube deformation on the applied force in the limit of large η is attributed to large amount of energy that is dissipated due to viscous forces in the highly occluded region, instead of doing mechanical work to deflect and expand the peak region of the tube.

In the occluded region away from $z = 3\pi/2$, the numerical solution in figure 9 suggests that the tube radius rapidly approaches zero with increasing η. This implies that keeping the dominant terms of (13) reduces to $a^2 = 1 - q$. The occluded region has a constant radius. In contrast to the previous problem inside a tube of type $n = 0$, in which q was determined by the occluded region, q in a tube of type $n = 4$ must be obtained by matching the occluded and peak regions using matched asymptotic expansions. It can be shown in the matched region near $z = 3\pi/2 \pm \eta^{-2/13}\delta$ that all terms are dominant in (13), except the contribution to dp/dz from $\eta \cos z$, which drops to leading order. A scaling analysis of the reduced equation of (13) and its boundary conditions in the matched region indicates that $1-q = o(\eta^{-35/26})$. The prefactor of this scaling is approximately 2.9 because numerical values of $(1-q)\eta^{35/26}$ quickly approach this value with increasing η. This theoretical prediction agrees well with numerical results as shown in figure 11. Note that the characteristic proportion of fluid left behind the wave approaches 0 more quickly in the limit of $\eta \to \infty$ in a tube of type $n = 4$ than $n = 0$. A tube of type $n = 4$ has a smaller occluded region

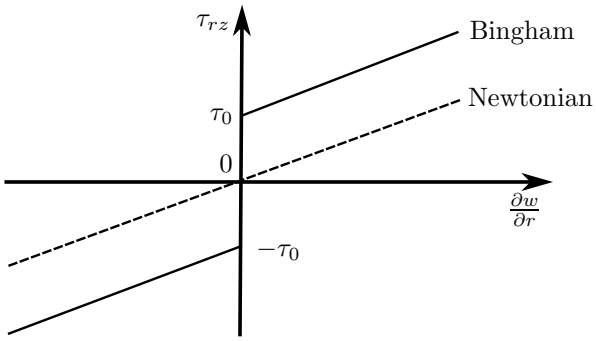

Figure 12: Stress-strain relationships of a Newtonian fluid and a Bingham plastic. The Newtonian curve has a slope corresponding to its viscosity. The Bingham curve has a stress-intercept corresponding to the yield stress and a slope corresponding to the plastic viscosity.

than a tube of type $n = 0$, implying a trapped core of larger size in the peak region that allows more fluid to propagate with the wave.

It has been determined that a non-zero radial force always results in deformation of a tube of Newtonian fluid. This is no longer the case when the tube contains fluid with a yield stress, where sufficient force on the tube must be applied to induce any motion. The problem of pumping a Bingham plastic, which is a type of non-Newtonian fluid with a yield stress, is considered in the following section. For simplicity, the tube is of type $n = 0$ in the remaining sections.

3 Bingham plastic

Consider a Bingham fluid with yield stress τ_0 and plastic viscosity μ. The Bingham fluid behaves either like a Newtonian fluid of viscosity μ in regions where the shear stress exceeds the yield stress, or like a plug without deformation in regions where the shear stress is below the yield stress. The stress-strain relationship of a Bingham fluid is compared with that of a Newtonian fluid in figure 12. The introduction of the yield stress modifies the force balance in the axial direction (9) to the system of equations

$$\frac{dp}{dz} = \frac{1}{r}\frac{\partial}{\partial r}\left(r\tau_{rz}\right) \tag{25}$$

and

$$\frac{\partial w}{\partial r} = \begin{cases} \tau_{rz} - sgn\left(\frac{\partial w}{\partial r}\right) B & |\tau_{rz}| > B, \\ 0 & |\tau_{rz}| < B, \end{cases} \tag{26}$$

where

$$B \equiv \frac{\tau_0 R}{\mu c} \tag{27}$$

is the dimensionless yield stress, also known as the Bingham number. Equation (26) is the one-dimensional approximation of the Bingham constitutive law that applies to the current problem in a slender geometry (Vajravelu et al., 2005). The limit as $B \to 0$ reduces to the Newtonian problem encountered in section 2.

The boundary conditions of the axial velocity w are the same as in the Newtonian problem. The solution, satisfying the no-slip condition on the tube wall and regularity at $r = 0$, is given by

$$w = \begin{cases} -\frac{1}{4}\frac{dp}{dz}[(a^2 - r^2) - 2r_0(a - r)] - 1 & r > r_0 \\ -\frac{1}{4}\frac{dp}{dz}(a - r_0)^2 - 1 & r \leq r_0, \end{cases} \tag{28}$$

where

$$r_0 = \min\left[2B/|dp/dz|, a\right] \tag{29}$$

is the radius of the plug-like region inside the tube. The velocity profile is either parabolic for $r > r_0$ or uniform for $r \leq r_0$. The central region of the tube, bounded by radius r_0, is actually a pseudo-plug because the associated velocity profile is flat in radius and only appears to be below the yield stress to leading order (Balmforth and Craster, 1999). Indeed, this region is not truly rigid because axial velocity variations remain, except if $r_0 = a$, in which case the fluid spanning that section of the tube becomes truly rigid.

The time-averaged flow rate in the lab frame, $q = 2\langle\int_0^a (w + 1)r\,dr\rangle$, is computed from the axial flow velocity w in the wave frame, as in section 2. The expression for q is given by

$$q = -\frac{1}{24}\frac{dp}{dz}(a - r_0)^2\left((a + r_0)^2 + 2a^2\right) - a^2 + 1, \tag{30}$$

where dp/dz is given by (8) with $n = 0$. The expression on the right hand side of (30) without the two final terms represents the steady flow rate in the wave frame and is equivalent to the Buckingham-Reiner equation (Bird et al., 1987). In the limit as $B \to 0$, the flow rate in (30) with $r_0 = 0$ reduces to (13) and recovers the flow rate of Newtonian fluid, as expected.

The tube radius is determined by solving the governing equations as a boundary-value problem in the domain $0 \leq z \leq 2\pi$. Equation (30), subject to the periodic boundary condition $a(0) = a(2\pi)$, contains an eigenvalue q and must be solved subject to the integral constraint (12). A sample solution is shown in figure 13 and features three qualitatively distinct regions. A sheared region, $r_0 < r < a$, forms near the tube wall where the tube is most deformed. A region of pseudo-plug, $r < r_0 < a$, forms inside the sheared region. A solid region, $r < r_0 = a$, occupies the entire cross-section of the tube where its radius is uniform in z. This means that at any extent along the tube in the lab frame, a stationary region develops during an interval of time, which begins after the departure of a sheared region and ends on arrival of another sheared region.

In the limit of small forcing amplitude η, solutions of the form $a = 1 + \eta a_1 + o(\eta^2)$ and $q = \eta^2 q_2 + o(\eta^3)$ are sought, as in section 2. In a tube of type $n = 0$

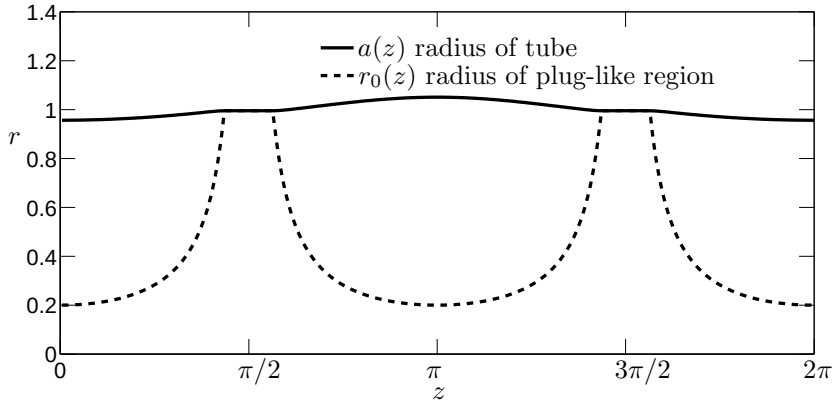

Figure 13: Numerical solution of the tube radius and the plug-like region inside a Bingham fluid. The input parameters are $n = 0$, $D = 0$, $\eta = 1$, $B = 0.1$.

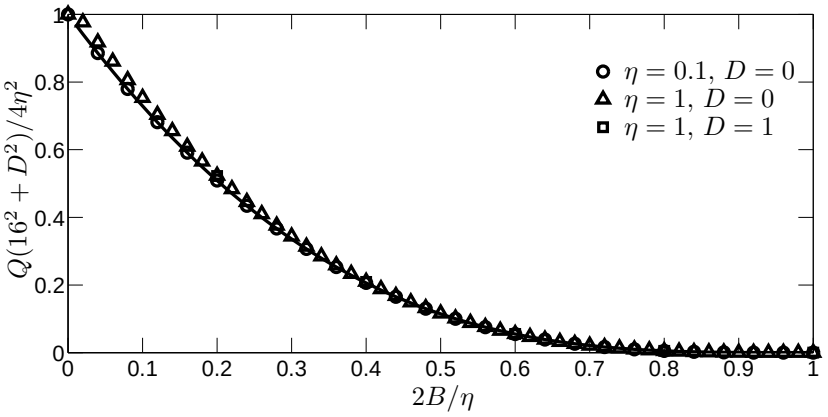

Figure 14: Theoretical prediction for small η and numerical solutions of the time-averaged flow rate of Bingham fluid, scaled by the corresponding flow rate of Newtonian fluid. The theoretical prediction is represented by the solid curve. The numerical solutions, represented by different symbols, are obtained by fixing η and varying the Bingham number given by (27) from 0 to $\eta/2$.

without stiffness, $D = 0$, it follows from (30) that

$$a = 1 - \frac{\eta}{48}\cos z(1 - r_0)^2\left((1 + r_0)^2 + 2a^2\right) + o(\eta^2). \tag{31}$$

The time-averaged flow rate q is computed by operating $\langle\cdot\rangle$ on (30), the method adopted in section 2. It can be shown, after some steps of algebra, that

$$q = \frac{\eta^2}{96}\langle\cos^2 z(1 - r_0)^3\left((1 + r_0)^2 + 2\right)\rangle. \tag{32}$$

There is no contribution to (32) from the solid region, where $r_0 = 1$. The flow rate is determined by the sheared regions, $|z| < \xi$ and $|z - \pi| < \xi$, where $\xi \equiv \cos^{-1}(2B/\eta)$ is the half-width of each region. Substituting $r_0 = 2B/\eta|\cos z|$ into (32) and integrating over the sheared regions gives

$$q = \frac{\eta^2}{48\pi}f(\xi), \tag{33}$$

where

$$\begin{aligned} f(\xi) \quad = \quad & \frac{3\xi}{2} - \frac{11}{4}\sin(2\xi) + 4\xi\cos^2\xi + \tan\xi\cos^4\xi \\ & - \cos^5\xi\left(\tanh^{-1}(\tan\frac{\xi}{2}) + \frac{1}{4(1 - \sin\xi)} - \frac{1}{4(\cos\frac{\xi}{2} + \sin\frac{\xi}{2})^2}\right) \end{aligned} \tag{34}$$

Figure 14 shows the flow rate given by (33), scaled by the corresponding flow rate of Newtonian fluid, (16), as a function of the rescaled Bingham number, $2B/\eta$. The theoretical prediction for $D = 0$ and small η is in excellent agreement with numerical results. The rescaled flow rate is a monotonically decreasing function of the rescaled Bingham number for $2B/\eta \leq 1$, as shown in figure 14, because the plug-like region increases in size and reduces the flow due to a larger yield stress. In the limit as $2B/\eta \to 1$, the flow rate $q \to 0$ because the forcing amplitude η is insufficient to drive much flow. For $2B/\eta \geq 1$, $q = 0$ because the yield stress is not overcome by the imposed force, resulting in no motion. As the Bingham number approaches 0, the flow rate given by (33) approaches the corresponding flow rate of Newtonian fluid, as expected.

In the limit of large forcing amplitude η, solutions are obtained by examining the flow near threshold of no motion, $a = r_0 = 1$, which occurs in the limit as $2B/\eta \to 1$. The small parameter $\epsilon \equiv 1 - 2B/\eta$ is introduced to examine the limit as $\epsilon \to 0$. Equations (29) and (30) respectively suggest solutions of the form $r_0 = 1 - \epsilon r_1 + o(\epsilon^2)$ and $a = 1 + \epsilon^2 a_2 + o(\epsilon^3)$. The $o(\epsilon)$ correction to the radius of the plug-like region

$$r_1 = \begin{cases} 1 - \frac{\zeta^2}{2} & |\zeta| < \sqrt{2},\ |\zeta - \epsilon^{-1/2}\pi| < \sqrt{2}, \\ 0 & \text{otherwise}, \end{cases} \tag{35}$$

where $\zeta = \epsilon^{-1/2}z$ is the rescaled axial coordinate, is obtained by expanding $\cos z$ near $z = 0, \pi$ in (29). Substituting r_1 into (30) gives

$$a_2 = \pm\frac{\eta r_1^2}{8}, \tag{36}$$

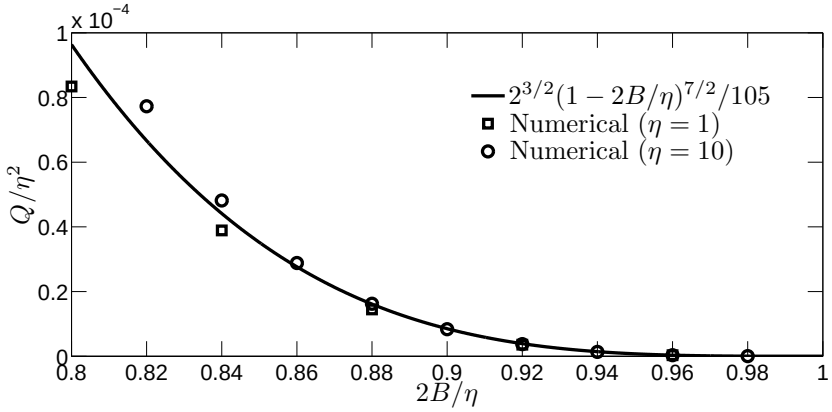

Figure 15: Theoretical prediction in the asymptotic limit as $2B/\eta \to 1$ and numerical solutions of the time-averaged flow rate of Bingham fluid.

where $\pm$ is either $+$ for $|\zeta| < \sqrt{2}$ or $-$ for $|\zeta - \epsilon^{-1/2}\pi| < \sqrt{2}$. Operating $\langle\cdot\rangle$ on (30) gives

$$q = \frac{2^{3/2}\eta^2\epsilon^{7/2}}{105}, \tag{37}$$

which is in agreement with numerical results as shown in figure 15. The flow rate scales like $\epsilon^{7/2}$, indicating that the flow of Bingham plastic increases very weakly with the applied force as it overcomes the yield stress.

It has been determined that the flow rate of both Newtonian fluid and Bingham fluid is a monotonically non-decreasing function of the forcing amplitude. This is no longer the case for the speed of propulsion of a rigid body inside a tube filled with fluid, as investigated in the following section.

4 Rigid body

Consider a rigid body of radius b surrounded by a Newtonian fluid of density ρ and dynamic viscosity μ. For simplicity, the rigid body is considered to be an infinitely-long rod of constant radius b so that steady and periodic solutions can be obtained in the wave frame. The rod has steady axial velocity W in the lab frame, as sketched in figure 16.

The axial velocity profile of the fluid is governed by (9), subject to no-slip conditions on the tube wall and the rigid rod. The boundary conditions that $w = 0$ on $r = a$ and $w = W$ on $r = b$ determine the axial velocity in the lab frame,

$$w = -\frac{1}{4}\frac{dp}{dz}(a^2 - r^2) - \left(\frac{W + \frac{1}{4}\frac{dp}{dz}(a^2 - b^2)}{\log\frac{a}{b}}\right)\log\frac{r}{a}. \tag{38}$$

In a similar manner to before in sections 2 and 3, the flow rate in the lab frame

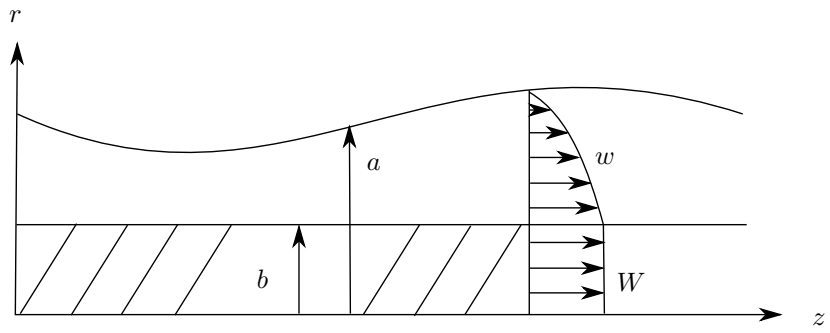

Figure 16: Schematic sketch in cylindrical polar coordinates of an elastic tube filled with Newtonian fluid and a rigid rod. The rod has radius b and propels at a steady axial velocity W in the lab frame.

is determined and given by

$$q = -\frac{1}{8}\frac{dp}{dz}\left(a^4 - b^4 - \frac{(a^2-b^2)^2}{\log(\frac{a}{b})}\right) + \frac{W(a^2-b^2)}{2\log(\frac{a}{b})} - b^2W - a^2 + 1. \qquad (39)$$

In the limit as $b \to 0$, the flow rate given by (39) reduces to the flow rate of Newtonian fluid without any rod given by (13), as expected. Note that the boundary-value problem governed by (39), with the same periodic boundary condition $a(0) = a(2\pi)$ as before, features W as an eigenvalue to be determined in addition to the eigenvalue q.

The two eigenvalues are determined by imposing two integral constraints, one of which is given by the global conservation of fluid, (12). Another integral constraint is obtained from the axial force balance on the rigid rod. Given that the rod is in steady motion, there is no net force exerted on the rod. This is written mathematically as $\langle [r\partial w/\partial r]_{r=b} \rangle = 0$, which reduces to

$$\langle \frac{W + \frac{1}{4}\frac{dp}{dz}(a^2-b^2)}{\log\frac{a}{b}} \rangle = 0. \qquad (40)$$

Figure 17 shows a set of solutions of tubes containing rigid rods of different size, where the forcing amplitude is fixed at $\eta = 10$. The associated eigenvalues, q and W, are presented later. The special case of $b = 0$ corresponds to a tube of Newtonian fluid only, which features an occluded region and a peak region, as investigated in section 2. The peak radius of the tube decreases with increasing b as shown in figure 17, indicating that the presence of the rigid rod reduces the deformation of the tube. The tube is occupied with more solid and less fluid, which partly explains the decreased deformation of the tube with increasing radius of the rigid rod.

The flow rate q increases with η in a qualitatively similar manner, independent of the rod radius b. However, the steady speed of the rod W increases for

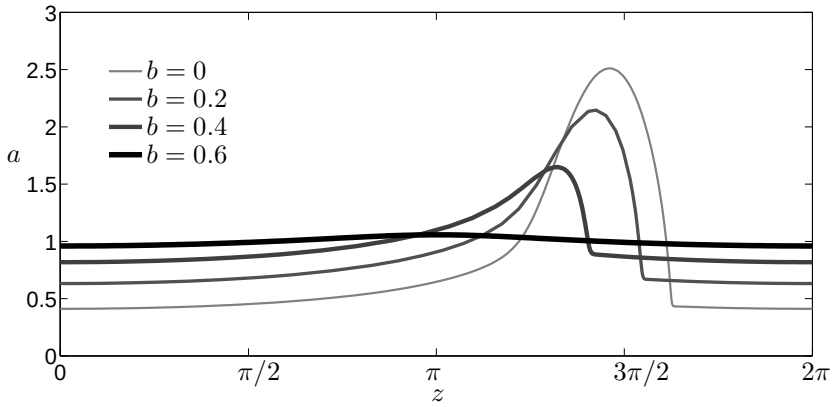

Figure 17: Numerical solutions of the deformed tube containing a rigid rod of different radius b, propelled by a radial force of amplitude $\eta = 10$.

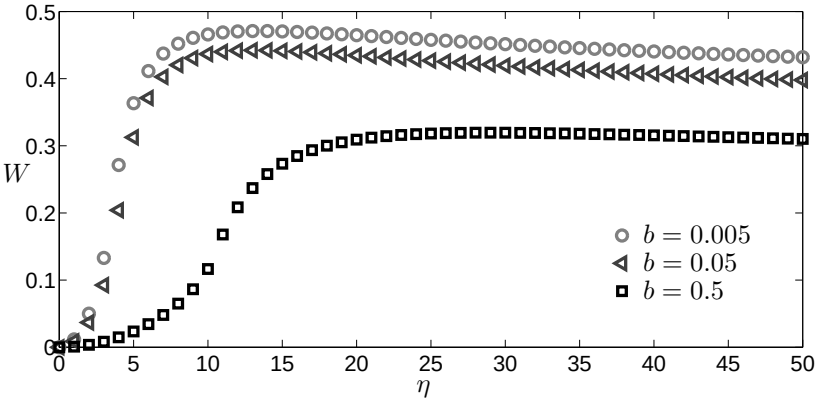

Figure 18: Numerical solutions of the steady velocity of the rigid rod of radius b as a function of the forcing amplitude η.

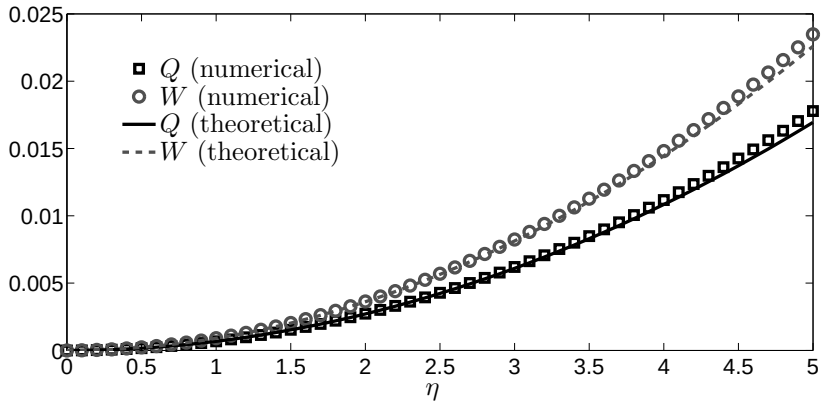

Figure 19: Theoretical predictions in the asymptotic limit of $\eta \to 0$ and numerical solutions of the flow rate q of fluid and the steady speed W of rigid body.

small η and decreases for large η, as shown in figure 18 for three representative values of b. For all values of rod radius, a maximal speed is attained at an intermediate value of η. The maximal attainable speed is less than half the wave speed. The rod speed decreases with η thereafter because the large forcing increases the viscous resistance in the occluded region, making it more difficult for the rod to move relative to the tube. The rod speed generally decreases with increasing b, indicating that it is more difficult to propel a rod of greater size. The quantitative details of the two asymptotic limits of small and large forcing amplitudes are investigated separately below.

In the limit of small η, solutions of the form $a = 1 + \eta a_1 + o(\eta^2)$, $q = \eta^2 q_2 + o(\eta^3)$, and $W = \eta^2 W_2 + o(\eta^3)$ are sought. Equation (39) to order η reduces to $kDda_1/dz + 16a_1 = -k\cos z$, which is integrated subject to the periodic boundary condition $a_1(0) = a_1(2\pi)$ to obtain the solution

$$a = 1 - \eta \frac{16k\cos z + k^2 D \sin z}{(kD)^2 + 16^2} + o(\eta^2), \tag{41}$$

where $k = 1 - b^4 + (1-b^2)^2/\log b$.

The solution given by (41) is substituted into the integral constraint (40) to obtain the leading-order speed of the rigid rod,

$$W = \frac{2k}{(kD)^2 + 16^2}\left(2 + \frac{1-b^2}{\log b}\right)\eta^2 + o(\eta^3). \tag{42}$$

Operating $\langle\cdot\rangle$ on (39) obtains the leading-order flow rate in the lab frame,

$$q = \frac{2k}{(kD)^2 + 16^2}\left(2 + \frac{1-b^2}{\log b}\right)(1-b^2)\eta^2 + o(\eta^3). \tag{43}$$

Note that $q \to W$ in the limit as $b \to 0$, indicating that a rigid wire of negligible radius propagates along the centreline of the tube at a steady speed correspond-

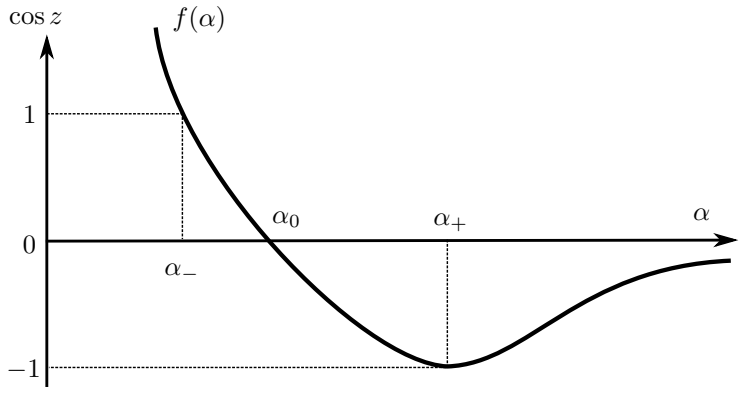

Figure 20: Sketch of $f(\alpha)$ given by (49), which changes sign at α_0 and attains its minimum of -1 at α_+. The value α_- corresponds to the minimal radius of the tube in the occluded region.

ing to the flow rate of the surrounding fluid. The solutions given by (42) and (43) are in agreement with numerical results, as shown in figure 19.

In the limit of large η, the resultant deformation of the tube is qualitatively similar to that of a tube containing Newtonian fluid only, as in section 2. A peak region near $z = 3\pi/2$ and an occluded region away from $z = 3\pi/2$ are expected to develop. The two regions are investigated separately below.

In the peak region near $z = 3\pi/2$, the peak radius is determined in a similar manner to before in section 2. The conditions in the peak region are that the pressure is uniform and that the total volume must be conserved by (12). The peak radius is given by

$$a_{max} = \left(\frac{15^2 \pi^2 (1-b^2)^2 \eta}{2^7 D^5} \right)^{1/5}, \tag{44}$$

which scales like $\eta^{1/5}$ with a prefactor that decreases with increasing b, in agreement with numerical results.

In the occluded region, the radius of the tube is expected to approach the radius of the rigid rod. Solutions of the form

$$a = b + \eta^{-1/2} \alpha + o(\eta^{-1}) \tag{45}$$

are sought, with the two eigenvalues of the form

$$W = W_\infty + o(\eta^{-1/2}) \tag{46}$$

and

$$q = 1 - b^2 - \eta^{-1/2} b \hat{q} + o(\eta^{-1}), \tag{47}$$

where α, W_∞ and $\hat{q}$ are all of order 1 to be determined. Note that $1 - b^2 - q$ is a measure of the proportion of fluid left behind the wave, which is expected

to scale like $(a-b)b$ and diminish in the limit as $\eta \to \infty$. This is because most of the fluid is trapped in a recirculating core of the peak region and propagates with the wave, while the remaining fluid lies in a thin shell of radius b and thickness $a-b$, the gap between the tube and the rod. The choice of the scaling $\eta^{-1/2}$ for corrections to a, q and W is justified below. A cubic equation for α,

$$\cos z\, \alpha^3 + 6(2 - W_\infty)\alpha - 6\hat{q} = 0, \tag{48}$$

is obtained by substituting (45), (46), and (47) into (39), and neglecting terms of order η^{-1}. All three terms in the cubic equation must be of order 1 by demanding that $a \to b + o(\eta^{-1/2})$, $q \to 1 - b^2 + o(\eta^{-1/2})$ and $W \to W_\infty + o(\eta^{-1/2})$, which justifies the earlier choice of the scaling $\eta^{-1/2}$. The solution for α is determined implicitly by a rearrangement of (48),

$$\cos z = f(\alpha) \equiv \frac{6}{\alpha^3}\left(\hat{q} - \alpha\,(2 - W_\infty)\right). \tag{49}$$

The function f has a local minimum at $\alpha_+ = 3\hat{q}/(4-2W_\infty)$ with the asymptotic limits that $f \to \infty$ as $\alpha \to 0$ and $f \to 0$ as $\alpha \to \infty$, as sketched in figure 20. Given that the tube radius must match smoothly with the peak region as $z \to 3\pi/2$, f must attain a local minimum of -1. The equation $f(\alpha_+) = -1$ reduces to

$$\hat{q} = \frac{2^{3/2}}{3}\,(2 - W_\infty)^{3/2}, \tag{50}$$

which provides an equation for the two unknown quantities, W_∞ and $\hat{q}$. A minimal tube radius is attained at $z = 0$, where $\alpha = \alpha_-$ satisfies the cubic equation $f(\alpha_-) = 1$. The function f changes sign at $\alpha_0 = 2\alpha_+/3$.

In addition to equation (50), another equation relating W_∞ and $\hat{q}$ can be obtained by (40). Note that contributions to the integral (40) from the occluded region are dominant because they are negligible from the peak region, where $a \sim \eta^{1/5}$ as $z \to 3\pi/2$. By substituting (45) into (40) and keeping only the leading-order terms of order $\eta^{1/2}$, we obtain

$$\langle \frac{2W_\infty}{\alpha} + \alpha \cos z \rangle = 0. \tag{51}$$

This integral constraint indicates that the tangential-stress balance is between the stress due to the rod speed and the radial forcing in the occluded region. The tangential stress on the rod is independent of the peak region or the stiffness D of the tube. Furthermore, the governing equations for W_∞ and $\hat{q}$, (50) and (51), are independent of b. This indicates that in the limit of large forcing amplitudes, the size of the rod does not influence its speed of propulsion to leading order. The integral constraint (51) reduces to

$$(4W_\infty - 6)\langle \alpha^{-1} \rangle + (4 - 2W_\infty)^{3/2} \langle \alpha^{-2} \rangle = 0, \tag{52}$$

by substituting (49) and (50) into (51). The integral $\langle \cdot \rangle$ in z-space can be evaluated in α-space by using (49), treating the three regions of $0 \le z \le \pi$,

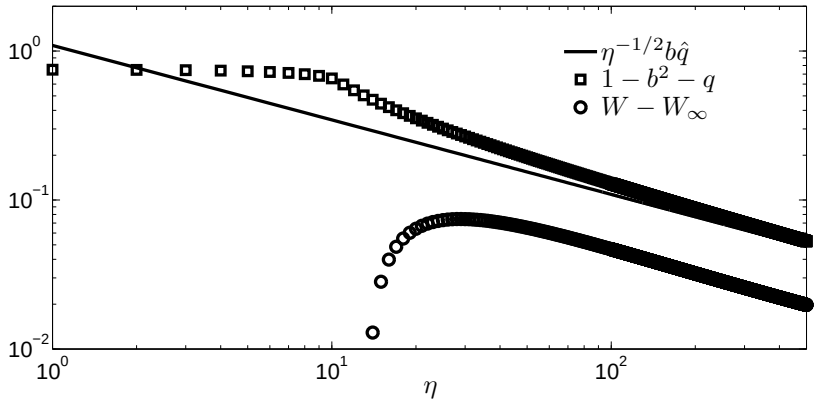

Figure 21: The proportion of fluid left by the wave $1-b^2-q$ and the approach of the rod speed W to $W_\infty \approx 0.247$ for large forcing amplitudes η, plotted on logarithmic scales. The radius of the rod $b = 0.5$ is fixed. Theoretical prediction for the proportion of fluid left by the wave, $\eta^{-1/2}b\hat{q}$, with $\hat{q} \approx 2.19$, agrees with numerical results. The slope of $W - W_\infty$ indicates that W approaches W_∞ like $\eta^{-1/2}$.

$\pi < z < 3\pi/2$ and $3\pi/2 < z < 2\pi$ separately. This gives

$$\langle \cdot \rangle = \int_{\alpha_+}^{\infty} \cdot J \, d\alpha - \int_{\alpha_-}^{\alpha_0} \cdot J \, d\alpha - \int_{\alpha_-}^{\alpha_+} \cdot J \, d\alpha, \tag{53}$$

where

$$J = \frac{df/d\alpha}{2\pi\sqrt{1-f^2}}. \tag{54}$$

Solving equation (52), where $\langle \alpha^{-1} \rangle$ and $\langle \alpha^{-2} \rangle$ are evaluated numerically using (53), gives $W_\infty \approx 0.247$. It follows that $\hat{q} \approx 2.19$ by (50) and completes the theoretical analysis of the problem.

A measure of the proportion of fluid left behind the wave is plotted as a function of the forcing amplitude in figure 21. Numerical values approach slowly to the theoretical prediction with increasing forcing amplitude. The difference between the rod speed from $W_\infty \approx 0.247$, also shown in figure 21, approaches 0 like $\eta^{-1/2}$, which is consistent with (46). In the limit of large forcing amplitude, most of the fluid is carried with the wave while the rod propels at approximately a quarter of the wave speed in the tube.

5 Conclusions

A theoretical analysis of fluid driven along a deformable tube by a prescribed radial force provides important insight into peristaltic motion. For small forcing amplitudes η, the deformation of the tube is of order η and the time-averaged

flow rate is of order η^2, independent of the three different types of fluid considered in the tube. For large forcing amplitudes η, different results are obtained depending on the contents of the tube, as summarised separately below.

A tube of Newtonian fluid features an occluded region and a peak region, where a trapped core of fluid recirculates in the wave frame. The peak region, which is shorter and more deformed in a linearly elastic tube with a spring constant D than a thin shell of constant bending stiffness D, depends importantly on the elastic properties of the tube and weakly on the forcing amplitude. A larger forcing amplitude increases the size of the trapped core in the peak region, allowing more fluid to propagate with the wave.

A tube of Bingham plastic features a sheared region, a pseudo-plug region, and a solid region in the wave frame, provided that the applied force has overcome the yield stress. The existence of the three distinct regions reduces the flow rate of the Bingham plastic considerably compared to that of a Newtonian fluid, which is sheared everywhere. The flow rate of the Bingham plastic increases from 0 extremely slowly with the forcing amplitude as the yield stress is overcome.

The steady propulsion of a rigid rod surrounded by Newtonian fluid in a tube shows that the size of the rod plays an important role. As the radius of the rod increases, the tube deforms less with a smaller speed of propulsion of the rod. The maximal speed of the rod, which is less than half the wave speed, is attained at a moderate forcing amplitude. A larger body, which reduces the maximal attainable speed of propulsion, is a bitter pill to swallow for the hungry python.

The propulsion of a rigid body in a deformable tube could be pursued further by modifying the underlying assumptions of the problem. The theoretical analysis presented here is limited to describing steady and periodic solutions in the wave frame. Time-dependent solutions in a non-periodic domain could be investigated, for example, by prescribing a radial force with a solitary-wave profile to drive a rigid body of finite length. This may provide further insight into the motion of the rigid body, where the regions ahead and behind the body in the tube are respectively relaxed and contracted.

Acknowledgements

The project was supervised by Neil Balmforth and undertaken as part of the Geophysical Fluid Dynamics program at the Woods Hole Oceanographic Institution. I benefited enormously from fruitful discussions with him at Walsh Cottage and on the soccer field. I also benefited from enjoyable discussions with other members of the program, including Joe Keller, John Wettlaufer, Jack Whitehead and Bill Young.

References

M. Argentina, J. Skotheim, and L. Mahadevan. Settling and swimming of flexible fluid-lubricated foils. *Physical Review Letters*, 99(22):224503, 2007.

N. J. Balmforth, D. Coombs, and S. Pachman. A stiff and slimy swimmer. *(submitted)*, 2009.

N. J. Balmforth and R. V. Craster. A consistent thin-layer theory for Bingham plastics. *Journal of Non-Newtonian Fluid Mechanics*, 84(1):65–81, 1999.

A. Bertuzzi, S. Salinari, R. Mancinelli, and M. Pescatori. Peristaltic transport of a solid bolus. *Journal of biomechanics*, 16(7):459, 1983.

R. B. Bird, R. C. Armstrong, and O. Hassager. Dynamics of polymeric liquids, Vol. 1, Fluid mechanics. *John Wiley& Sons, New York*, 1987.

J. G. Brasseur, S. Corrsin, and N. Q. Lu. Influence of a peripheral layer of different viscosity on peristaltic pumping with Newtonian fluids. *Journal of Fluid Mechanics*, 174:495–519, 1987.

E. O. Carew and T. J. Pedley. An active membrane model for peristaltic pumping: part I – Periodic activation waves in an infinite tube. *Journal of biomechanical engineering*, 119:66, 1997.

I. A. Frigaard and D. P. Ryan. Flow of a visco-plastic fluid in a channel of slowly varying width. *Journal of Non-Newtonian Fluid Mechanics*, 123(1): 67–83, 2004.

A. E. H. Love. *A treatise on the mathematical theory of elasticity.* Dover Publications, 1944.

P.S. Lykoudis and R. Roos. The fluid mechanics of the ureter from a lubrication theory point of view. *Journal of Fluid Mechanics*, 43(04):661–674, 1970.

A. H. Shapiro, M. Y. Jaffrin, and S. L. Weinberg. Peristaltic pumping with long wavelengths at low Reynolds number. *Journal of Fluid Mechanics*, 37, 1969.

K. Vajravelu, S. Sreenadh, and V. Ramesh Babu. Peristaltic transport of a Herschel–Bulkley fluid in an inclined tube. *International Journal of Non-Linear Mechanics*, 40(1):83–90, 2005.

J. S. Wettlaufer and M. G. Worster. Dynamics of premelted films: frost heave in a capillary. *Physical Review E*, 51(5):4679–4689, 1995.

J. S. Wettlaufer, M. G. Worster, L. A. Wilen, and J. G. Dash. A theory of premelting dynamics for all power law forces. *Physical review letters*, 76(19): 3602–3605, 1996.